Light-tunable three-phase coexistence in mixed halide perovskites

DOI:
[10.1103/PhysRevB.106.134110](https://doi.org/10.1103/PhysRevB.106.134110)

Document status and date:
Published: 01/10/2022

Document Version:
Publisher's PDF, also known as Version of Record (includes final page, issue and volume numbers)

Please check the document version of this publication:

• A submitted manuscript is the version of the article upon submission and before peer-review. There can be important differences between the submitted version and the official published version of record. People interested in the research are advised to contact the author for the final version of the publication, or visit the DOI to the publisher's website.
• The final author version and the galley proof are versions of the publication after peer review.
• The final published version features the final layout of the paper including the volume, issue and page numbers.

Link to publication

Light-tunable three-phase coexistence in mixed halide perovskites

Zehua Chen [1,2] Geert Brocks [1,2,3] Shuxia Tao [1,2,*] and Peter A. Bobbert [2,4,†]

[1]*Materials Simulation and Modelling, Department of Applied Physics, Eindhoven University of Technology,*
5600 MB Eindhoven, The Netherlands

[2]*Center for Computational Energy Research, Department of Applied Physics, Eindhoven University of Technology,*
P. O. Box 513, 5600 MB Eindhoven, The Netherlands

[3]*Computational Materials Science, Faculty of Science and Technology and MESA+ Institute for Nanotechnology,*
University of Twente, P. O. Box 217, 7500 AE Enschede, The Netherlands

[4]*Molecular Materials and Nanosystems, Eindhoven University of Technology,*
P. O. Box 513, NL-5600 MB Eindhoven, The Netherlands

Mixed iodine-bromine perovskites used in solar cells undergo below a critical temperature an intrinsic demixing into phases with different iodine-bromine compositions. In addition, under illumination they show nucleation of an iodine-rich phase. We predict from thermodynamic considerations that in mixed iodine-bromine perovskites like $MAPb(I_{1-x}Br_x)_3$ the interplay of these effects can lead to coexistence of a bromine-rich, iodine-rich, and nearly iodine-pure nucleated phase. This three-phase coexistence occurs in a region in the composition-temperature phase diagram near the critical point for intrinsic demixing. We investigate the hysteresis in the evolution of this coexistence when temperature or illumination intensity are cycled. Depending on the particular way the coexistence is established, nearly iodine-pure nuclei should form either in the iodine-rich phase only or both in the bromine-rich and iodine-rich phases. Experimental verification of this fundamentally novel type of light-tunable three-phase coexistence should be possible by a combination of absorption and photoluminescence experiments.

I. INTRODUCTION

The interest in the fundamental physical processes of metal-halide perovskites is rapidly increasing because of their spectacular performance in photovoltaic and light emission applications [1–9]. One of these processes is halide segregation in mixed halide perovskites. Such perovskites have the unique feature that their band gap can be tuned by varying the halide concentration ratio. This tunability can be exploited to optimize the optoelectronic performance of all-perovskite multijunction solar cells [10,11] or tandem solar cells consisting of a silicon bottom cell and a perovskite top cell [9,12]. Halide segregation is a serious. problem in such applications and fundamental understanding of this process is therefore of utmost importance.

Apart from its importance for developing efficient solar cells, halide segregation is a very interesting fundamental physical phenomenon in itself. The different halide ions can be viewed as particles of different substances that prefer to mix or demix, following fundamental thermodynamical laws. In particular, minimization of the Helmholtz free energy, consisting of an enthalpic and an entropic contribution, determines if a mixed or demixed state is preferred. The enthalpic contribution favors demixing while the entropic contribution favors mixing, and the competition between the two determines the preference for mixing or demixing. In the extensively studied mixed halide perovskite $MAPb(I_{1-x}Br_x)_3$ (MA stands for the organic cation methylammonium) this leads to a miscibility gap, i.e., a range of halide composition values $x_1 < x < x_2$ for which there is no stable mixture below a critical temperature T_c [13]. Such a miscibility gap had been predicted from a computational investigation within density-functional theory combined with a thermodynamic analysis [14]. The resulting composition-temperature, x-T, phase diagram is similar to the well-known phase diagram of a binary mixture, where a binodal signals that the free energy of the demixed situation becomes lower than that of the mixed situation, and a spinodal signals the disappearance a free-energy barrier between the mixed and demixed situation. The binodal and spinodal meet at the critical point (x_c, T_c). Above the critical temperature T_c no demixing occurs because the entropic contribution to the free energy then always dominates.

What makes the halide segregation process especially interesting, and very different from demixing processes in ordinary binary mixtures, is the fact that it can be influenced by light. Even when the mixed state of a perovskite like $MAPb(I_{1-x}Br_x)_3$ is stable in the dark, low-band gap iodine-rich nuclei are formed under illumination [15–17]. Since a return to the original mixed situation occurs when illumination is interrupted, the effect should have a thermodynamic origin. The effect was rationalized by funneling of photocarriers, generated by illumination of the perovskite film, into these nuclei [17]. The nuclei originate from random composition

---

*S.X.Tao@tue.nl
†P.A.Bobbert@tue.nl

fluctuations that tend to grow by inward diffusion of iodine ions and outward diffusion of bromine ions, a process that is driven by the energy gain of the photocarriers funneling into the low-band gap nuclei. When the illumination is interrupted, the driving force for the growth of the nuclei disappears and the fully mixed situation is gradually restored. A complete thermodynamic theory for the effect should not only consider the compositional free energy governing halide segregation in the dark, but also the free energy of the photocarriers redistributing by diffusion over the different phases. We recently made a first step in constructing such a theory, where the key element is the consideration of the *sum* of the compositional and photocarrier free energy, and minimization of this total free energy for a situation of two coexisting phases with different halide composition [18]. When the total free energy of the two coexisting phases is lower than that of a single mixed phase, the demixed situation is preferred. With this analysis, we could explain various experimental observations on light-induced halide segregation [6,15,16,19–24].

However, a major puzzle remained unsolved, namely the possible formation by halide segregation of *three* coexisting phases with different halide compositions. Such a situation could be compared to the well-known gas-liquid-solid coexistence occurring in many substances, like water, where the volume fraction of water molecules is different in the gas, liquid, and solid phase. Demonstration of such a three-phase coexistence would therefore not only shed further light on halide segregation in mixed halide perovskites but also be of foundational interest.

An indication for such a three-phase coexistence is the finding in our previous analysis of a compositional and a light-induced binodal that meet at a "triple point" (x_{tr}, T_{tr}), with x_{tr} and T_{tr} depending on the illumination intensity I [18]. The compositional binodal signals halide segregation into a bromine-rich and an iodine-rich phase, whereas the light-induced binodal signals the nucleation of a nearly iodine-pure phase from a mixed phase by the illumination. A three-phase coexistence of an iodine-rich, bromine-rich, and nearly iodine-pure phase at (x_{tr}, T_{tr}) may thus be expected. However, if such three-phase coexistence would only occur at (x_{tr}, T_{tr}), then experimental observation of this phenomenon would be extremely difficult. It would require searching for a line in a three-dimensional (x, T, I) phase space, where changing x would involve fabricating a range of perovskite samples with different iodine-bromine composition. On the other hand, if there would be a sufficiently large three-dimensional region in (x, T, I) phase space with three-phase coexistence, instead of only a line, then experimental verification would be much easier. Because all present considerations of halide segregation are limited to two coexisting phases, this question could up to now not be addressed.

To address this question, we present in this work a thermodynamic theory for light-tunable halide segregation in mixed iodine-bromine perovskites that considers the possible coexistence of *three* phases. We apply our theory to MAPb(I$_{1-x}$Br$_x$)$_3$ and show that an intriguingly rich phase diagram is obtained, with two new types of binodal-spinodal combinations signaling different types of transitions from two-phase to three-phase coexistence. Most importantly, we show that an extended and experimentally accessible region of

three-phase coexistence of an iodine-rich, bromine-rich, and nearly iodine-pure phase exists in (x, T, I) phase space near the critical point (x_c, T_c) for intrinsic demixing in the dark.

Section II explains the theoretical methodology that we followed, with technical details given in Appendices A–C. In Sec. III the general features of the predicted three-phase phase coexistence are discussed. Phase diagrams of MAPb(I$_{1-x}$Br$_x$)$_3$ for different illumination intensities are given and the three-phase coexistence is analysed in depth. We end with an outlook and a discussion in Sec. IV.

II. THEORETICAL METHODOLOGY

The key element of the theory is the minimization of a free energy consisting of the sum over the different phases of a compositional and a photocarrier free energy:

$$\Delta F^\star(\{x\}, \{\phi\}, T) = \sum_i \phi_i[\Delta F(x_i, T) + n_i E_g(x_i)]. \quad (1)$$

Here $\Delta F(x_i, T)$ is the compositional Helmholtz mixing free energy per formula unit (f.u.), x_i the bromine concentration, and ϕ_i the volume fraction of phase $i = 1, 2, 3$. Demanding local charge neutrality, the densities of photogenerated electrons and holes in each phase i are both given by n_i, the photocarrier density per f.u. The diffusion lengths of photocarriers are very long in perovskites and expected to be larger than the feature sizes of the different phase domains. An equilibrium photocarrier distribution over the different phases is therefore assumed obeying Boltzmann statistics. Since in practice $n_i \ll 1$, we can neglect state filling effects and use the Boltzmann factor $\exp[-E_g(x_i)/k_B T]$ in the statistical weighting, where $k_B T$ is the thermal energy, so that we have

$$n_i/n_j = e^{-[E_g(x_i) - E_g(x_j)]/k_B T}, \quad (2)$$

where $E_g(x)$ is the band gap at Br concentration x. Neglecting the small differences in the volume V per f.u. in the different phases, we have $\sum_i \phi_i = 1$ and $\sum_i \phi_i x_i = x$. In equilibrium, the total generation rate of photocarriers is equal to the total annihilation rate:

$$G = \sum_i \phi_i(n_i/\tau + k n_i^2/V), \quad (3)$$

where we make the simplifying assumption that the generation rate per f.u. G and the monomolecular and bimolecular recombination rates $1/\tau$ and k are the same in all phases. For the photocarrier generation rate in a thin perovskite film we take $G = I\alpha V/h\nu$, where I is the illumination intensity, α the absorption coefficient, and $h\nu$ the photon energy. We take the values $\tau = 100$ ns for the monomolecular recombination time and $k = 10^{-10}$ cm^3 s^{-1}, applicable for a standard MAPbI$_3$ film [25], $V = 2.5 \times 10^{-22}$ cm^3/f.u. [18], $\alpha = 10^5$ cm^{-1}, and $h\nu = 3$ eV [17]. The dependence of the band gap of MAPb(I$_{1-x}$Br$_x$)$_3$ on x has been experimentally determined and can be well described by the function $E_g(x) = 1.57 + 0.39x + 0.33x^2$ eV [26], interpolating between the band gap of 1.57 eV for MAPbI$_3$ and 2.29 eV for MAPbBr$_3$.

Regarding the calculation of the compositional free energy $\Delta F(x_i, T)$, we follow the procedure outlined in Ref. [14], as we also did in our previous analysis [18]. Considering exclusively the compositional free energy, only two-phase
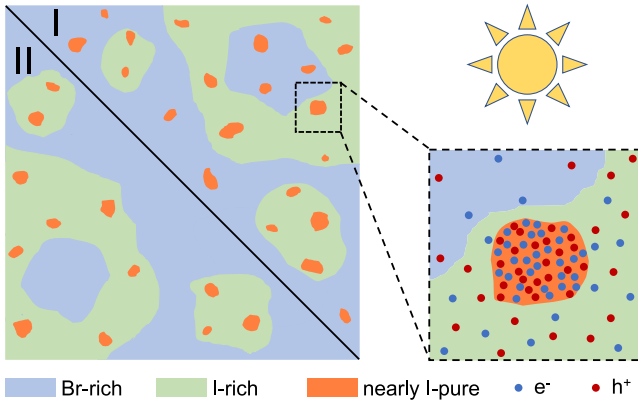
FIG. 1. Two types (I and II) of light-tunable three-phase coexistence in mixed I-Br perovskites. Blue: Br-rich phase. Green: I-rich phase. Orange: Nearly I-pure nuclei. The nearly I-pure nuclei can be present in (I) both the I-rich and Br-rich phase or (II) only in the I-rich phase. Magnification: funneling of photogenerated electrons and holes into the low-band gap nearly I-pure nuclei, reducing their free energy.

coexistence can occur. A phase diagram similar to that of an ordinary binary mixture is then obtained, with a binodal and a spinodal [14]. Figure 4 in Appendix A reproduces the compositional mixing free energy $\Delta F(x, T)$ of MAPb(I$_{1-x}$Br$_x$)$_3$ calculated in Ref. [18] for different temperatures T. We will use this free energy also in the present work.

All results presented in this work are based on minimization of the total free energy $\Delta F^\star(\{x\}, \{\phi\}, T)$ in Eq. (1) with respect to the ϕ_i's and x_i's. The technical aspects of finding the free-energy minima, establishing the character of these minima and their appearance and disappearance, which determine the locations of the various binodals and spinodals in the x-T phase diagram, are given in Appendices B–D. The related problems are fundamentally different from usual phase coexistence problems, where the free energy is the addition of the free energies of the different phases. This is not the case for the free-energy Eq. (1), because the photocarrier free energy $\phi_i n_i E_g(x_i)$ in phase i depends on the volume fractions of the other phases via Eqs. (2) and (3). We note that our equilibrium thermodynamic theory cannot make predictions about the sizes and distributions of domains of the different phases. Such information can only be obtained from a kinetic nonequilibrium theory.

III. RESULTS

Figure 1 illustrates the main findings of the present work when considering minimization of the sum of the compositional and photocarrier free energy in the presence of illumination when allowing for the coexistence of three phases. As in the dark, a decomposition into a Br-rich and an I-rich phase can take place, governed by the compositional free energy. At the same time, a lowering of the photocarrier free energy drives the light-induced formation of nearly I-pure nuclei. We will show that the interplay of these processes gives rise to two types of three-phase coexistence, with the nearly I-pure nuclei being present in (I) both the I-rich and B-rich phase or (II) only the I-rich phase. For definite-

ness, the labels "Br-rich," "I-rich," and "nearly I-pure" are used for phases for which $x_{\text{Br-rich}} > x_{\text{I-rich}} > x_{\text{nearly I-pure}}$, and $x_{\text{nearly I-pure}} \ll 1$.

We consider the phase diagrams of MAPb(I$_{1-x}$Br$_x$)$_3$ for different illumination intensities I. Binodals and spinodals are found by determining the minima of the total free energy. As usual, a binodal signals the crossing of the free energies of the global and a local free-energy minimum and therefore a change of the character of the global free-energy minimum. A spinodal signals the vanishing of a local minimum and hence the vanishing of a free-energy barrier between two local minima.

Figures 2(a)–2(c) show the phase diagrams of MAPb(I$_{1-x}$Br$_x$)$_3$ for illumination intensities I corresponding to 2, 20, and 200 Sun ($I = 100$ mW cm$^{-2} = 1$ Sun), obtained from our previous analysis, which assumed possible coexistence of not more than two phases [18]. The blue and green curves indicate the compositional and light-induced binodals, respectively, where the mixed situation (white) becomes metastable for a transition to two-phase coexistence (gray). The red curve indicates the spinodal, where the free-energy barrier between the mixed and two-phase coexistence situations disappears. In our previous analysis we suggested that at the junction between the compositional and light-induced binodal [arrow in Fig. 2(a)] three-phase coexistence might occur [18].

Figures 2(d)–2(f) show the phase diagrams when possible coexistence of three phases is taken into account. Next to the binodals in Figs. 2(a)–2(c), two new binodals (orange curves) appear, signaling that the free-energy minimum of a three-phase coexistence as illustrated in Fig. 1 becomes lower than that of two-phase coexistence. Because there are two types of two-phase coexistence, there are also two types of binodals, signaling a transition from (1) two-phase coexistence of nuclei of a nearly I-pure phase and an I-Br mixed phase to three-phase coexistence, and (2) two-phase coexistence of an I-rich and Br-rich phase to three-phase coexistence. Each of the two binodals is accompanied by a spinodal that signals the disappearance of the free-energy barrier between the corresponding two-phase and three-phase coexistence minima. Figures 2(g)–2(i) zoom in to the three-phase coexistence regions, where the pairs of binodals and spinodals are labeled accordingly by "1" and "2." The spinodals continue in the two-phase coexistence regions, where they signal the disappearance of free-energy barriers between the two types of two-phase coexistence (not shown). The interpretation of the different regions indicated in the phase diagrams Figs. 2(d)–2(i) is the following. In the white region called "mixed," the fully mixed situation has the lowest free energy and no demixing occurs. In the gray region called "nearly I-pure + mixed," the lowest free-energy minimum corresponds to a situation where there is a small volume fraction of light-induced nearly I-pure nuclei in a mixed I-Br parent phase. In the gray region called "I-rich + Br-rich," the lowest free-energy minimum corresponds to a situation with compositional demixing into an I-rich and a Br-rich phase. The three-phase coexistence can arise from both of these two-phase coexistence situations. In the area delineated by the orange lines (the binodals for two-phase to three-phase coexistence), the situation with three-phase coexistence of nearly I-pure nuclei coexisting with an I-rich
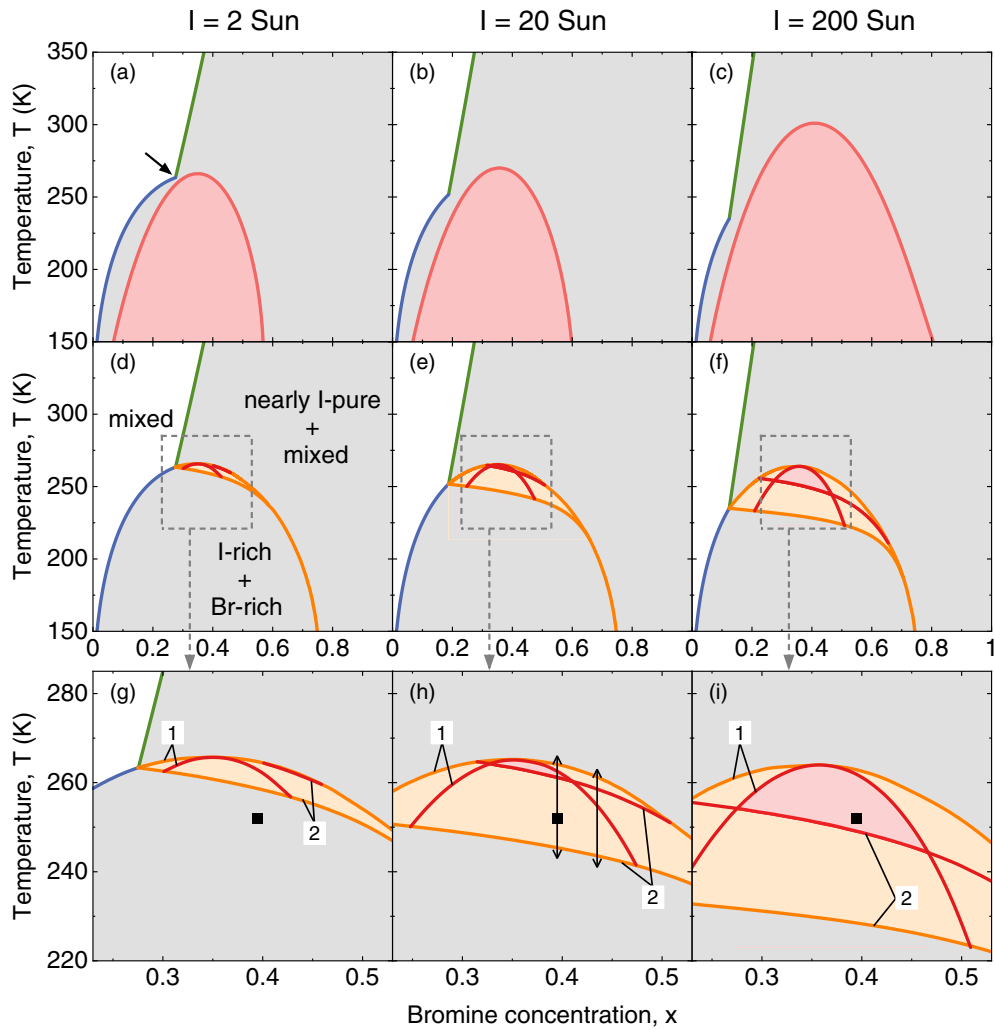
FIG. 2. [(a)–(c)] Phase diagrams of MAPb($I_{1-x}Br_x$)$_3$ for different illumination intensities when accounting for coexistence of not more than two phases. Blue curve: Compositional binodal. Green curve: Light-induced binodal. Red curve: Spinodal. Arrow in (a): Suggested "triple point" for three-phase coexistence. [(d)–(f)] Phase diagrams when accounting for coexistence of three phases. Orange curves: Binodals for transitions from the two types of two-phase coexistence to three-phase coexistence. Red curves: Corresponding spinodals. Yellow (pink) region: Two-phase coexistence partly (fully) unstable for formation of third phase. [(g)–(i)] Magnifications of three-phase coexistence regions with labeling of binodal-spinodal pairs for the two types of transitions. Double-headed arrows in (h): Temperature ranges and Br concentrations x in Figs. 3(a) (left arrow) and (b) (right arrow). Black squares in (g)–(i): Temperature T and Br concentration x in Fig. 3(c).

phase and a Br-rich phase has a lower free energy than that of either of the two-phase coexistence situations. When crossing the upper binodal, labeled "1," the three-phase coexistence is reached from the nearly I-pure + mixed" coexistence, while when crossing the lower binodal, labeled "2," the three-phase coexistence is reached from the "I-rich + Br-rich" coexistence. We will see further on that in these two cases we reach the three-phase coexistence of situations I and II, respectively, in Fig. 1. Although in the area delineated by the spinodals the situation with three-phase coexistence has a lower free energy than the two situations with two-phase coexistence, the free-energy energy barrier between the two situations with two-phase coexistence and three-phase coexistence only disappears when crossing the corresponding spinodal. Therefore, only in the region in between spinodals "1" and "2" [the pink region in Figs. 2(e), 2(f) 2(h), and 2(i)] the three-phase coexistence arises spontaneously.

The main conclusion from the phase diagrams is that a sizable three-phase coexistence region exists in (x, T, I) phase space near the critical point (x_c, T_c) for intrinsic halide demixing in the dark. The critical point following from our calculations is $(x_c, T_c) = (0.35, 266$ K); see Fig. 4 in Appendix A. In case of a compositional free energy that is symmetric in the two phases, the critical Br concentration would be $x_c = 0.5$. However, Fig. 4 shows a strong asymmetry, leading to a significant deviation from $x_c = 0.5$. Such asymmetry also occurs in other A-site perovskites, like FAPb($I_{1-x}Br_x$)$_3$ (FA: formamidinium) and MA$_{7/8}$Cs$_{1/8}$Pb($I_{1-x}Br_x$)$_3$ [18].

We observe in Figs. 2(e), 2(f) 2(h), and 2(i) that the two types of spinodals may cross. In an experiment investigating the three-phase coexistence, two situations may therefore occur when decreasing or increasing T, indicated by the two
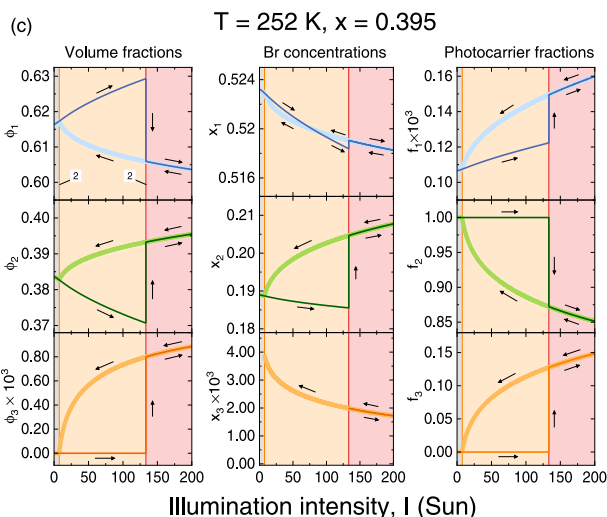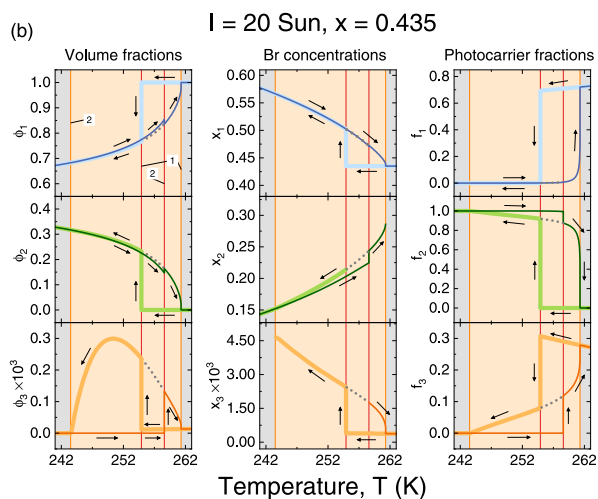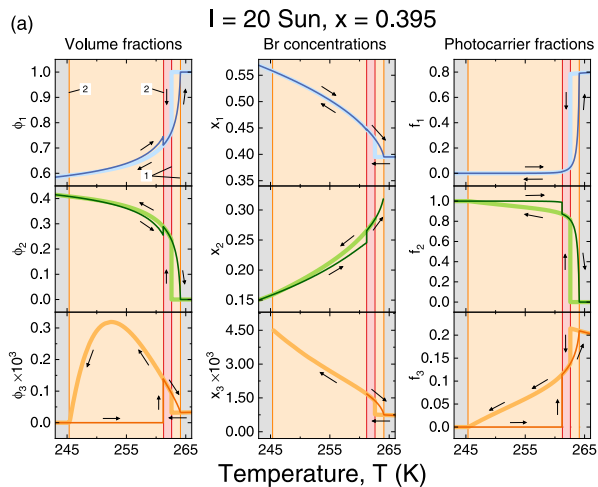
(a) I = 20 Sun, x = 0.395

(b) I = 20 Sun, x = 0.435

(c) T = 252 K, x = 0.395

FIG. 3. Volume fractions ϕ_i, bromine concentrations x_i, and photocarrier fractions f_i as function of temperature T at illumination intensity $I = 20$ Sun for (a) $x = 0.395$ [path forth and back along left double-headed arrow in Fig. 2(h)] and (b) $x = 0.435$ [path forth and back along right double-headed arrow in Fig. 2(h)]. From top to bottom: Br-rich phase ($i = 1$), I-rich phase ($i = 2$), and nearly I-pure phase ($i = 3$). Thin (thick) dark-colored (light-colored) lines: Increasing (decreasing) T. Free-energy minima are followed until they disappear. The different regions and binodals and spinodals crossed
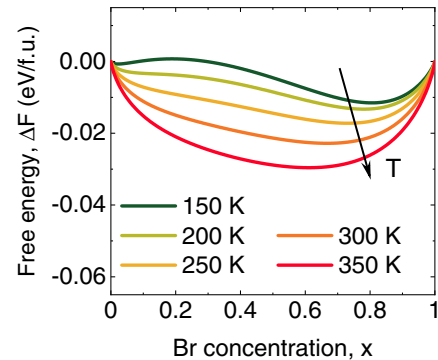

FIG. 4. Compositional mixing free energy per formula unit (f.u.) as a function of Br concentration x at different temperatures T. Reproduced from Ref. [18].

double-headed arrows at $x = 0.395$ and 0.435 in Fig. 2(h). Figures 3(a) and 3(b) show, for these two compositions and an illumination intensity $I = 20$ Sun, results for the volume fractions ϕ_i and Br concentrations x_i of the three phases, and the photocarrier fractions $f_i = \phi_i n_i / \sum_i \phi_i n_i$ in these phases. In plotting these results it is assumed that, after crossing a binodal when decreasing or increasing T, the system makes a transition to three-phase coexistence only after crossing the corresponding spinodal, because only then the free-energy barrier for this transition has disappeared. The resulting supercooling or superheating leads to the hysteresis in the plots. We observe that volume fractions of about 0.03% of the nearly I-pure phase can be reached, with a maximum Br concentration of about 0.45% and a photocarrier fraction of 20-30%. The fact that the very small volume fraction of the nearly I-pure phase contains a relatively large fraction of the photocarriers is a consequence of the very strong effect of funneling of photocarriers into this phase. The fundamental difference between the two situations depicted in Figs. 3(a) and 3(b) is that in Fig. 3(a) a temperature range (pink) exists where the transition to the three-phase coexistence always occurs, while in Fig. 3(b) the transition requires overcoming a free-energy barrier. The three-phase coexistence is then both for decreasing and increasing T "hidden" behind this barrier, as indicated by the dotted lines in Fig. 3(b).

The situation depicted as "I" in Fig. 1, with nearly I-pure nuclei in both the I-rich and Br-rich phase, can only arise when entering the three-phase coexistence region by decreasing T. The mixed I-Br phase in which the nearly I-pure nuclei are embedded then decomposes into an I-rich and a Br-rich phase; see Appendix D. By contrast, when entering the three-phase coexistence region by increasing T, the nearly I-pure nuclei are exclusively generated in the I-rich phase (situation "II" in Fig. 1).

are indicated with the same colors as in Figs. 2(d)–2(i). The dotted lines in (b) indicate that the three-phase coexistence is separated from the two types of two-phase coexistence by a free-energy barrier. The labels "1" and "2" indicate the binodal-spinodal pairs also indicated in Figs. 2(g)–2(i). (c) Same as (a) and (b) but as function of I for $T = 252$ K and $x = 0.395$ [black squares in Figs. 2(g)–2(i)]. Thin (thick) dark-colored (light-colored) lines: Increasing (decreasing) I.

In between each binodal and its corresponding spinodal, the barrier for the formation of a third phase is determined by the free energy required to generate a critical nucleus of the third phase in either of the two existing phases. This barrier is, in the absence of defects and impurities, governed by an interface free energy. Determination of this interface free energy is beyond the scope of the present work. In practice defects and impurities might dominate the nucleation process, preventing supercooling and superheating. In that case the binodals and not the spinodals delineate the region where three-phase coexistence will be found experimentally.

We conclude by showing in Fig. 3(c) similar results as in Figs. 3(a) and 3(b) but now for varying illumination intensity I for $T = 252$ K and $x = 0.395$ [black squares in Figs. 2(g)–2(i)]. A large hysteresis loop is observed that starts at 8 Sun, featuring "superillumination" until 133 Sun, where the nearly I-pure phase spontaneously appears with a volume fraction of about 0.08% and Br concentration of about 0.2%, containing about 13% of the photocarriers. The same remarks as above about a free-energy barrier to form a critical nucleus for the nearly I-pure phase apply to this situation. As is clear from Figs. 2(g)–2(i), the way in which the three-phase coexistence region is entered for increasing I is the same as for increasing T. This means that the nearly I-pure nuclei are in this case exclusively generated in the I-rich phase (situation "II" in Fig. 1).

One can obtain an effective photocarrier lifetime from $\tau_{\mathrm{eff}} = n/G$, where $n = \sum_i \phi_i n_i$ is the number of photocarriers per f.u. averaged over the phases present in the perovskite. Halide segregation will change τ_{eff} because it leads to a non-homogeneous distribution of photocarriers over the different phases. This changes the amount of photocarriers lost by bimolecular recombination due its quadratic dependence on the photocarrier density. To investigate this effect, we consider as an example the point ($x = 0.395$, $T = 252$ K, $I = 20$ Sun) in phase space, indicated by the black square in Fig. 2(h). If no halide segregation would occur, then we have $\tau_{\mathrm{eff}} = 76$ ns [obtained by solving n from Eq. (3) for the case of a single phase: $G = n/\tau + kn^2/V$]. The deviation from the monomolecular recombination time $\tau = 100$ ns is caused by the bimolecular recombination. For the cases of two- and three-phase coexistence, we find $\tau_{\mathrm{eff}} = 39$ and 41 ns, respectively [from the data for the thin dark-colored and thick light-colored lines, respectively, in Fig. 3(a) for $T = 252$ K]. So the two-phase segregation into an I-rich phase [$x = 0.19$, see the thin dark-colored line in middle panel of middle column of Fig. 3(a) for $T = 252$ K] and a Br rich phase ($x = 0.52$, same but upper panel) leads to a reduction of τ_{eff} by almost a factor of 2. This reduction is caused by the enhanced bimolecular recombination in the I-rich phase, where the photocarrier density is increased. Interestingly, the further segregation to three-phase coexistence, with nucleation of a nearly I-pure phase ($x = 3.2 \times 10^{-3}$, see lowest panel of middle column in Fig. 3(a) for $T = 252$ K), slightly increases τ_{eff} from 39 to 41 ns.

IV. SUMMARY, OUTLOOK, AND DISCUSSION

By considering the sum of a compositional and photocarrier free energy, we have found that the mixed halide perovskite MAPb($\mathrm{I}_{1-x}\mathrm{Br}_x$)$_3$ can show light-tunable three-phase coexistence in a region in the composition-temperature, x-T, phase diagram close to the critical point (x_c, T_c) for halide segregation in the dark. The three coexisting phases are a Br-rich, an I-rich, and a nucleated nearly I-pure phase. We have determined the binodals and spinodals for the transition to this three-phase coexistence either from a two-phase coexistence of a mixed I-Br phase and a light-induced nucleated nearly I-pure phase or from a two-phase coexistence of a Br-rich and an I-rich phase. In the transition to three-phase coexistence from two-phase coexistence of a mixed I-Br phase and a light-induced nucleated nearly I-pure phase, the nearly I-pure nuclei will be present in both the Br-rich and the I-rich phase. In the transition to three-phase coexistence from two-phase coexistence of a Br-rich and an I-rich phase, the nuclei will only be present in the I-rich phase.

Although we focused on a particular mixed halide perovskite, MAPb($\mathrm{I}_{1-x}\mathrm{Br}_x$)$_3$, and used particular parameter values, we expect that the concepts developed in this work will be applicable to mixed halide perovskites in general. We stress that substantial uncertainties in our quantitative predictions are expected, because we had to make several simplifying assumptions. Quantitative improvements of our work in several directions are possible. Accounting for different monomolecular and bimolecular recombination rates in the different phases will be relatively easy, but the information required for this is presently not available to us. Accounting for nonuniformity of the photocarrier distribution inside the phase domains will be more complicated, requiring information about the diffusion lengths of the photocarriers in comparison to the sizes and shapes of the domains. We further remark that we have applied thermodynamic equilibrium arguments, which cannot account for kinetic effects. One such effect is the kinetic trapping of Br ions inside the nearly I-pure nuclei [27], possibly explaining why the observed Br concentration of $x \approx 0.2$ in these nuclei [15] is not as small as expected from equilibrium arguments. Finally, when changing temperature, perovskites may undergo structural phase transitions and volume changes that will interfere with halide segregation. Nevertheless, we expect the three-phase coexistence to be a robust phenomenon, also present in quantitatively improved versions of our analysis. In particular, we expect that our conclusion that the light-tunable three-phase coexistence should occur close to the critical point for intrinsic halide segregation in the dark will be unaffected by quantitative improvements.

We propose experimental verification of the predicted three-phase coexistence by a combination of absorption and photoluminescence experiments. Presence of both the I-rich and Br-rich phase can be detected by the occurrence of two steplike increases at the respective band gaps in the absorption spectrum. The additional nearly I-pure phase can be detected by a peak in the photoluminescence spectrum close to the band gap of MAPbI$_3$. Because of the funneling effect, a sizable peak should be visible, despite the very small volume fraction of this phase. As discussed at the end of the previous section, halide segregation will be accompanied by a change of the effective photocarrier lifetime, which can be detected by time-resolved photoluminescence experiments. We remark that extreme illumination intensities are not needed. We studied three-phase coexistence in Figs. 3(a) and 3(b) for $I =$

20 Sun, but it is also present at $I = 2$ Sun [see Figs. 2(d) and 2(g)] and even lower illumination intensities.

A worry could be that experimental verification requires cooling down to temperatures around T_c, where slowing down of halide diffusion might hamper observation. Estimates of the diffusion barriers for vacancy-mediated diffusion of I and Br in $MAPb(I_{1-x}Br_x)_3$ are 0.17–0.25 and 0.23–0.43 eV, respectively [28]. Taking 0.25 eV as a typical barrier and an Arrhenius T dependence, we find that the diffusion speed is slowed down by a factor of about 3 at the calculated $T_c = 266$ K [18] as compared to room temperature and by a somewhat larger factor well within the three-phase coexistence region. Since light-induced halide demixing at room temperature occurs on timescales of hours [29], establishing equilibrium conditions for three-phase coexistence should still occur on experimentally feasible timescales. $MAPb(I_{1-x}Br_x)_3$ seems a good candidate for experimental verification, since the calculated T_c's of other $AB(I_{1-x}Br_x)_3$ perovskites are lower [18]. We mention in this context that the precise value of the calculated T_c depends rather sensitively on technical details of the calculations. For example, in Ref. [14] a value $T_c = 343$ K was reported for $MAPb(I_{1-x}Br_x)_3$, which is even above room temperature. Considerable uncertainties in calculated values of T_c should therefore be expected.

Experimental verification of the three phase coexistence would establish a fundamentally novel type of three-phase coexistence and provide a new viewing angle on demixing processes in mixed halide perovskites. The tunability by light makes the present three-phase coexistence fundamentally different from gas-liquid-solid coexistence as occurring, e.g., at the triple point of water. The insight that light can be used as a parameter to influence segregation processes can possibly also be applicable to other compound semiconductors where the band gap changes with composition.

APPENDIX A: COMPOSITIONAL MIXING FREE ENERGY

In Fig. 4 we reproduce the compositional mixing free energy $\Delta F(x, T)$ calculated in Ref. [18] that enters Eq. (1). This mixing free energy was calculated following the procedure outlined in Ref. [14], using density-functional theory with a thermodynamic analysis performed within the generalized quasichemical approximation [30].

APPENDIX B: BINODALS AND SPINODALS FOR THE TRANSITION FROM THE MIXED PHASE TO TWO-PHASE COEXISTENCE

We apply Eqs. (1)–(3) to the case of halide segregation into two phases. Substituting n_1 and n_2, which can be obtained by solving Eqs. (2) and (3), Eq. (1) becomes

$$
\Delta F^\star(x_1, x_2, \phi_1, \phi_2, T) = \phi_1 \Delta F(x_1) + \phi_2 \Delta F(x_2)
$$
$$
+ 2G\tau \frac{\phi_1 f(x_1) + \phi_2 f(x_2)}{\phi_1 g(x_1) + \phi_2 g(x_2) + \sqrt{[\phi_1 g(x_1) + \phi_2 g(x_2)]^2 + D[\phi_1 g^2(x_1) + \phi_2 g^2(x_2)]}}, \tag{B1}
$$

with

$$
D = 4Gk\tau^2/V, \tag{B2}
$$

and

$$
f(x) = E_g(x) e^{-E_g(x)/k_B T},
$$
$$
g(x) = e^{-E_g(x)/k_B T}. \tag{B3}
$$

The T dependence in Eq. (B1) has been suppressed. We should minimize Eq. (B1) under the conditions $\phi_1 + \phi_2 = 1$ and $\phi_1 x_1 + \phi_2 x_2 = x$.

To find the binodals in the x-T phase diagram, we investigate the possibility, starting from the mixed situation with Br concentration x, to decrease the free energy by demixing through nucleation of a phase with a Br concentration $x_2 \neq x$ with a small volume fraction $\delta\phi \equiv \phi_2$. The free energy, Eq. (B1), in the mixed situation is $\Delta F^\star(x, x, 1, 0, T)$, while the free energy in the demixed situation is $\Delta F^\star(x_1, x_2, 1 - \delta\phi, \delta\phi, T)$, with, to linear order in $\delta\phi$, $x_1 = x - (x_2 - x)\delta\phi$. The difference in free energy between the demixed and mixed situations is to linear order in $\delta\phi$:

$$
\delta\Delta F^\star = \delta\phi \left[\Delta F(x_2) - \Delta F(x) + (x - x_2)\Delta F'(x) + 2G\tau \left(\frac{f(x_2) - f(x) + (x - x_2)f'(x)}{(1 + \sqrt{1 + D})g(x)} \right. \right.
$$
$$
- \frac{f(x)}{[(1 + \sqrt{1 + D})g(x)]^2} \left\{ g(x_2) - g(x) + (x - x_2)g'(x) \right.
$$
$$
\left. \left. \left. + \frac{2g(x)(g(x_2) - g(x) + (x - x_2)g'(x)) + D[g^2(x_2) - g^2(x) + 2(x - x_2)g(x)g'(x)]}{2\sqrt{1 + D}g(x)} \right\} \right) \right]. \tag{B4}
$$

When $\delta\Delta F^\star < 0$, the demixed situation has a lower free energy than the mixed situation. We therefore find the binodals in Figs. 2(a)–2(c) for a certain illumination intensity I by looking if a value x_2 of a nucleated phase exists for which $\delta\Delta F^\star = 0$.

To find the spinodals we consider the possibility to decrease the free energy by generating a volume fraction ϕ of a phase with a slightly different concentration $x_2 = x + \delta x$. The free energy in the demixed situation can be written as $\Delta F^\star(x - \phi\delta x/(1 - \phi), x + \delta x, 1 - \phi, \phi, T)$. To second order in δx the difference in free energy becomes

$$\delta\Delta F^\star = \frac{\phi(\delta x)^2}{2(1-\phi)}\left\{\Delta F''(x) + 2G\tau\left[\frac{f''(x)}{(1+\sqrt{1+D})g(x)} - \frac{f(x)}{[(1+\sqrt{1+D})g(x)]^2}\left(g''(x)\right.\right.\right.$$
$$\left.\left.\left. + \frac{g(x)g''(x) + D\{[g'(x)]^2 + g(x)g''(x)\}}{\sqrt{1+D}g(x)}\right)\right]\right\}. \tag{B5}$$

Putting $\delta\Delta F^\star = 0$ yields the spinodal separating the unstable from the metastable region in the x-T phase diagrams shown in Figs. 2(a)–2(c).

We remark that Eqs. (B4) and (B5) are more accurate than Eqs. (11) and (13) in Ref. [18]. Equations (B4) and (B5) consider bimolecular recombination in both the parent and nucleated phases while Eqs. (11) and (13) in Ref. [18] neglect bimolecular recombination in the parent phase. For the illumination intensities studied in Ref. [18] this is a good approximation, but in the present work this not a good approximation anymore for an illumination intensity of 200 Sun.

APPENDIX C: EXTENSION OF THE COMMON TANGENT METHOD

The binodals also follow from demanding that $\partial\Delta F^\star/\partial x_2 = 0$ and $\partial\Delta F^\star/\partial\phi_2 = 0$ under the conditions $\phi_1 + \phi_2 = 1$ and $\phi_1 x_1 + \phi_2 x_2 = x$, with $\Delta F^\star$ given by Eq. (B1). When only considering the compositional free energy this leads to the common tangent equations $\Delta F(x_2) = \Delta F(x_1) - (x_1 - x_2)\Delta F'(x_1)$ and $\Delta F'(x_2) = \Delta F'(x_1)$. With the inclusion of the photocarrier free energy we obtain instead

$$\Delta F(x_2) = \Delta F(x_1) - (x_1 - x_2)\Delta F'(x_1) - 2G\tau\left\{\frac{f(x_2) - f(x_1) + (x_1 - x_2)f'(x_1)}{\phi_1 g(x_1) + \phi_2 g(x_2) + H_0}\right.$$
$$\left. - \frac{\phi_1 f(x_1) + \phi_2 f(x_2)}{(\phi_1 g(x_1) + \phi_2 g(x_2) + H_0)^2}\left[g(x_2) - g(x_1) + (x_1 - x_2)g'(x_1) + \frac{H_1}{2H_0}\right]\right\}, \tag{C1}$$

and

$$\Delta F'(x_2) = \Delta F'(x_1) - 2G\tau\left\{\frac{f'(x_2) - f'(x_1)}{\phi_1 g(x_1) + \phi_2 g(x_2) + H_0} - \frac{\phi_1 f(x_1) + \phi_2 f(x_2)}{(\phi_1 g(x_1) + \phi_2 g(x_2) + H_0)^2}\left[g'(x_2) - g'(x_1) + \frac{H_2}{2H_0}\right]\right\}, \tag{C2}$$

where H_0, H_1, and H_2 are

$$H_0 = \sqrt{[\phi_1 g(x_1) + \phi_2 g(x_2)]^2 + D[\phi_1 g^2(x_1) + \phi_2 g^2(x_2)]},$$
$$H_1 = 2[\phi_1 g(x_1) + \phi_2 g(x_2)][g(x_2) - g(x_1) + (x_1 - x_2)g'(x_1)]$$
$$\quad + D[g^2(x_2) - g^2(x_1) + 2g(x_1)g'(x_1)(x_1 - x_2)],$$
$$H_2 = 2[\phi_1 g(x_1) + \phi_2 g(x_2)][g'(x_2) - g'(x_1)] + 2D[g(x_2)g'(x_2) - g(x_1)g'(x_1)]. \tag{C3}$$

Putting $\phi_1 = 1 - \delta\phi$, $\phi_2 = \delta\phi$, and $x_1 = x - (x_2 - x)\delta\phi$ in Eq. (C1) and linearizing in $\delta\phi$ yields Eq. (B4).

APPENDIX D: BINODALS AND SPINODALS FOR THE TRANSITION FROM TWO-PHASE TO THREE-PHASE COEXISTENCE

To determine the binodals for the transition from two-phase to three-phase coexistence, we start with finding the minimum of the two-phase free energy in the metastable (gray) and unstable (pink) regions of the phase diagrams Figs. 2(a)–2(c), using a standard minimization algorithm. From this, the free energies $\Delta F^\star$, volume fractions ϕ_1 and ϕ_2, and Br concentrations x_1 and x_2 of the local and global minima are determined. The comparison of the free energies of the global minima leads to two distinct two-phase coexistence regions, separated by purple lines, as shown in Fig. 5 for MAPb(I$_{1-x}$Br$_x$)$_3$ at different illumination intensities. In the upper right region we have "nearly I-pure + mixed" coexistence and in the lower left region "I-rich + Br-rich" coexistence.

To determine the binodals we consider the possibility, starting from the free energy of the global two-phase coexistence minimum, to further decrease the free energy by generating a third phase with Br concentration $x_3 \neq x_1, x_2$ with a small volume fraction $\delta\phi \equiv \phi_3$. The two-phase free energy is obtained from Eq. (B1) and the three-phase free energy is $\Delta F^\star(x_1 + c_1\delta\phi,$
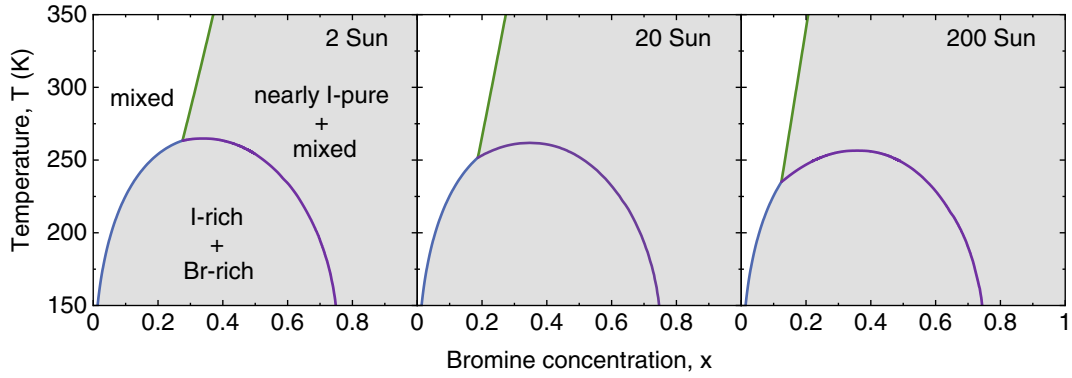
FIG. 5. Phase diagrams for two-phase coexistence in MAPb($I_{1-x}Br_x$)$_3$ at different illumination intensities. The purple lines indicate where the free-energy minima of the two different types of two-phase coexistence switch order.

$x_2 + c_2\delta\phi, x_3, \phi_1 - c\delta\phi, \phi_2 - (1-c)\delta\phi, \delta\phi, T$), with, to linear order in $\delta\phi$,

$$c_1\phi_1 + c_2\phi_2 - cx_1 - (1-c)x_2 + x_3 = 0, \tag{D1}$$

where c_1, c_2, and c are constants. The free-energy difference between the three-phase and two-phase coexistence is to linear order in $\delta\phi$:

$$\delta\Delta F^\star = \delta\phi\Bigg((c_1\phi_1\Delta F'(x_1) + c_2\phi_2\Delta F'(x_2) - c\Delta F(x_1) - (1-c)\Delta F(x_2) + \Delta F(x_3))$$

$$+ 2G\tau\Bigg\{\frac{c_1\phi_1 f'(x_1) + c_2\phi_2 f'(x_2) - cf(x_1) - (1-c)f(x_2) + f(x_3)}{\phi_1 g(x_1) + \phi_2 g(x_2) + H_0}$$

$$- \frac{\phi_1 f(x_1) + \phi_2 f(x_2)}{(\phi_1 g(x_1) + \phi_2 g(x_2) + H_0)^2}\Bigg[c_1\phi_1 g'(x_1) + c_2\phi_2 g'(x_2) - cg(x_1) - (1-c)g(x_2) + g(x_3) + \frac{H_3}{2H_0}\Bigg]\Bigg\}\Bigg), \tag{D2}$$

where

$$H_3 = 2[\phi_1 g(x_1) + \phi_2 g(x_2)][c_1\phi_1 g'(x_1) + c_2\phi_2 g'(x_2) - cg(x_1) - (1-c)g(x_2) + g(x_3)]$$

$$+ D(2c_1\phi_1 g(x_1)g'(x_1) + 2c_2\phi_2 g(x_2)g'(x_2) - cg^2(x_1) - (1-c)g^2(x_2) + g^2(x_3)). \tag{D3}$$

Since ϕ_1, ϕ_2, x_1, and x_2 are determined by minimizing the two-phase free energy, Eqs. (C1) and (C2) should be satisfied when inserting the numerically determined values. This means that we can substitute Eqs. (C1) and (C2) in Eq. (D2) to eliminate the constants c_1, c_2, and c. This leads to

$$\delta\Delta F^\star = \delta\phi\Bigg\{\Delta F(x_3) - \Delta F(x_1) + (x_1 - x_3)F'(x_1)$$

$$+ 2G\tau\Bigg[\frac{f(x_3) - f(x_1) + (x_1 - x_3)f'(x_1)}{\phi_1 g(x_1) + \phi_2 g(x_2) + H_0} - \frac{\phi_1 f(x_1) + \phi_2 f(x_2)}{(\phi_1 g(x_1) + \phi_2 g(x_2) + H_0)^2}\Big(g(x_3) - g(x_1) + (x_1 - x_3)g'(x_1)$$

$$+ \{2[\phi_1 g(x_1) + \phi_2 g(x_2)][g(x_3) - g(x_1) + (x_1 - x_3)g'(x_1)]$$

$$+ D[g^2(x_3) - g^2(x_1) + 2(x_1 - x_3)g(x_1)g'(x_1)]\}/2H_0\Big)\Bigg]\Bigg\}. \tag{D4}$$

When $\delta\Delta F^\star < 0$, the three-phase coexistence has a lower free energy than the two-phase coexistence. We thus find the binodals for the transition from two-phase to three-phase coexistence in Figs. 2(d)–2(i) by looking if a value x_3 of a third phase exists for which $\delta\Delta F^\star = 0$. Because we have two types of two-phase coexistence, we find two types of binodals. The binodals labeled "1" are those for the transition from "nearly I-pure + mixed" to three-phase coexistence and the binodals labeled "2" are those for the transition from "I-rich + Br-rich" to three-phase coexistence.

To find the spinodals we consider the possibility to decrease the free energy by generating a small volume fraction $\delta\phi_3$ of a third phase from the first phase with a slightly different Br concentration $x_3 = x_1 + \delta x_3$ (the argument is the same for generation of the third phase from the second phase). The free energy for the three-phase coexistence can be written as $\Delta F^\star(x_1 + \delta x_1, x_2 + \delta x_2, x_1 + \delta x_3, \phi_1 + \delta\phi_1, \phi_2 + \delta\phi_2, \delta\phi_3, T)$ with

$$\delta\phi_1 + \delta\phi_2 + \delta\phi_3 = 0, \tag{D5}$$

and

$$x_1\delta\phi_1 + x_2\delta\phi_2 + x_1\delta\phi_3 + \phi_1\delta x_1 + \phi_2\delta x_2 + \delta\phi_1\delta x_1 + \delta\phi_2\delta x_2 + \delta\phi_3\delta x_3 = 0. \tag{D6}$$

Taking $x_3 = x_1 + \delta x_3$, the free-energy difference between the three-phase and two-phase coexistence is to second order in δx_3:

$$
\begin{aligned}
\delta\Delta F^\star = {} & \Delta F(x_1)\delta\phi_1 + \Delta F(x_2)\delta\phi_2 + \Delta F(x_1)\delta\phi_3 + \phi_1\Delta F'(x_1)\delta x_1 + \phi_2\Delta F'(x_2)\delta x_2 \\
& + \Delta F'(x_1)\delta\phi_1\delta x_1 + \Delta F'(x_2)\delta\phi_2\delta x_2 + \Delta F'(x_1)\delta\phi_3\delta x_3 + \Delta F''(x_1)\delta\phi_3(\delta x_3)^2/2 \\
& + 2G\tau\Bigg\{\frac{1}{\phi_1 g(x_1) + \phi_2 g(x_2) + H_0}\Bigg[f(x_1)\delta\phi_1 + f(x_2)\delta\phi_2 + f(x_1)\delta\phi_3 \\
& + \phi_1 f'(x_1)\delta x_1 + \phi_2 f'(x_2)\delta x_2 + f'(x_1)\delta\phi_1\delta x_1 + f'(x_2)\delta\phi_2\delta x_2 + f'(x_1)\delta\phi_3\delta x_3 \\
& + f''(x_1)\delta\phi_3(\delta x_3)^2/2\Bigg] - \frac{\phi_1 f(x_1) + \phi_2 f(x_2)}{[\phi_1 g(x_1) + \phi_2 g(x_2) + H_0]^2}\Bigg[g(x_1)\delta\phi_1 + g(x_2)\delta\phi_2 \\
& + g(x_1)\delta\phi_3 + \phi_1 g'(x_1)\delta x_1 + \phi_2 g'(x_2)\delta x_2 + g'(x_1)\delta\phi_1\delta x_1 + g'(x_2)\delta\phi_2\delta x_2 \\
& + g'(x_1)\delta\phi_3\delta x_3 + g''(x_1)\delta\phi_3(\delta x_3)^2/2 + \frac{H_4}{2H_0}\Bigg]\Bigg\},
\end{aligned}
\tag{D7}
$$

where

$$
\begin{aligned}
H_4 = {} & 2[\phi_1 g(x_1) + \phi_2 g(x_2)][g(x_1)\delta\phi_1 + g(x_2)\delta\phi_2 + g(x_1)\delta\phi_3 + \phi_1 g'(x_1)\delta x_1 + \phi_2 g'(x_2)\delta x_2 \\
& + g'(x_1)\delta\phi_1\delta x_1 + g'(x_2)\delta\phi_2\delta x_2 + g'(x_1)\delta\phi_3\delta x_3 + g''(x_1)\delta\phi_3(\delta x_3)^2/2] \\
& + D(g^2(x_1)\delta\phi_1 + g^2(x_2)\delta\phi_2 + g^2(x_1)\delta\phi_3 + 2(\phi_1 g(x_1)g'(x_1)\delta x_1 + \phi_2 g(x_2)g'(x_2)\delta x_2 \\
& + g(x_1)g'(x_1)\delta\phi_1\delta x_1 + g(x_2)g'(x_2)\delta\phi_2\delta x_2 + g(x_1)g'(x_1)\delta\phi_3\delta x_3 \\
& + \{[g'(x_1)]^2 + g(x_1)g''(x_1)\}\delta\phi_3(\delta x_3)^2/2)).
\end{aligned}
\tag{D8}
$$

Substituting Eqs. (C1) and (C2) in Eq. (D7), the difference in free energy becomes

$$
\begin{aligned}
\delta\Delta F^\star = {} & \frac{1}{2}\delta\phi_3(\delta x_3)^2\Bigg\{\Delta F''(x_1) + 2G\tau\Bigg[\frac{1}{\phi_1 g(x_1) + \phi_2 g(x_2) + H_0}f''(x_1) \\
& - \frac{\phi_1 f(x_1) + \phi_2 f(x_2)}{[\phi_1 g(x_1) + \phi_2 g(x_2) + H_0]^2}\Bigg(g''(x_1) + \frac{[\phi_1 g(x_1) + \phi_2 g(x_2)]g''(x_1) + D\{[g'(x_1)]^2 + g(x_1)g''(x_1)\}}{H_0}\Bigg)\Bigg]\Bigg\}.
\end{aligned}
\tag{D9}
$$

Starting in the "nearly I-pure + mixed" coexistence region and decreasing T we first cross binodal "1." After that, the three-phase coexistence free energy becomes lower than the two-phase coexistence free energy, while a barrier between these free energies still exists. Taking x_1 as the Br concentration in the mixed phase, the barrier disappears when $\delta\Delta F^\star = 0$, which is where spinodal "1" is located. Taking instead x_1 as the Br concentration in the nearly I-pure phase, we have $\delta\Delta F^\star > 0$, demonstrating that the I-rich and Br-rich phase are generated from the mixed phase and not from the nearly I-pure phase. Vice versa, starting in the "I-rich + Br-rich" coexistence region and increasing T we first cross binodal "2." Taking x_1 as the Br concentration in the I-rich phase, the barrier disappears when $\delta\Delta F^\star = 0$, which is where spinodal "2" is located. Taking instead x_1 as the Br concentration in the Br-rich phase, we have $\delta\Delta F^\star > 0$, demonstrating that the nearly I-pure phase is generated from the I-rich phase and not from the Br-rich phase. The results in Fig. 3 have been obtained with a standard numerical minimization algorithm.

---

[1] A. Kojima, K. Teshima, Y. Shirai, and T. Miyasaka, J. Am. Chem. Soc. **131**, 6050 (2009).

[2] M. A. Green, A. Ho-Baillie, and H. J. Snaith, Nat. Photon. **8**, 506 (2014).

[3] N. K. Noel, S. D. Stranks, A. Abate, C. Wehrenfennig, S. Guarnera, A. A. Haghighirad, A. Sadhanala, G. E. Eperon, S. K. Pathak, M. B. Johnston, A. Petrozza, L. M. Herz, and H. J. Snaith, Energy Environ. Sci. **7**, 3061 (2014).

[4] S. D. Stranks and H. J. Snaith, Nat. Nanotechnol. **10**, 391 (2015).

[5] N. J. Jeon, J. H. Noh, W. S. Yang, Y. C. Kim, S. Ryu, J. Seo, and S. I. Seok, Nature (Lond.) **517**, 476 (2015).

[6] D. P. McMeekin, G. Sadoughi, W. Rehman, G. E. Eperon, M. Saliba, M. T. Hörantner, A. Haghighirad, N. Sakai, L. Korte, B. Rech, M. B. Johnston, L. M. Herz, and H. J. Snaith, Science **351**, 151 (2016).

[7] K. Lin, J. Xing, L. N. Quan, F. P. G. de Arquer, X. Gong, J. Lu, L. Xie, W. Zhao, D. Zhang, C. Yan, W. Li, X. Liu, Y. Lu, J. Kirman, E. H. Sargent, Q. Xiong, and Z. Wei, Nature (Lond.) **562**, 245 (2018).

[8] E. H. Jung, N. J. Jeon, E. Y. Park, C. S. Moon, T. J. Shin, T. Y. Yang, J. H. Noh, and J. Seo, Nature (Lond.) **567**, 511 (2019).

[9] A. Al-Ashouri, E. Köhnen, B. Li, A. Magomedov, H. Hempel, P. Caprioglio, J. A. Márquez, A. B. M. Vilches, E. Kasparavicius, J. A. Smith, N. Phung, D. Menzel, M. Grischek, L. Kegelmann, D. Skroblin, C. Gollwitzer, T. Malinauskas, M. Jošt, G. Matič, B. Rech et al., Science **370**, 1300 (2020).

[10] K. Xiao, J. Wen, Q. Han, R. Lin, Y. Gao, S. Gu, Y. Zang, Y. Nie, J. Zhu, J. Xu, and H. Tan, ACS Energy Lett. **5**, 2819 (2020).

[11] J. Wang, V. Zardetto, K. Datta, D. Zhang, M. M. Wienk, and R. A. J. Janssen, Nat. Commun. **11**, 5254 (2020).

[12] F. Fu, J. Li, T. C.-J. Yang, H. Liang, A. Faes, Q. Jeangros, C. Ballif, and Y. Hou, Adv. Mater. **34**, 2106540 (2022).

[13] F. Lehmann, A. Franz, D. Többens, S. Levcenco, T. Unold, A. Taubert, and S. Schorr, RSC Adv. **9**, 11151 (2019).

[14] F. Brivio, C. Caetano, and A. Walsh, J. Phys. Chem. Lett. **7**, 1083 (2016).

[15] E. T. Hoke, D. J. Slotcavage, E. R. Dohner, A. R. Bowring, H. I. Karunadasa, and M. D. McGehee, Chem. Sci. **6**, 613 (2015).

[16] R. E. Beal, D. J. Slotcavage, T. Leijtens, A. R. Bowring, R. A. Belisle, W. H. Nguyen, G. F. Burkhard, E. T. Hoke, and M. D. McGehee, J. Phys. Chem. Lett. **7**, 746 (2016).

[17] S. Draguta, O. Sharia, S. J. Yoon, M. C. Brennan, Y. V. Morozov, J. M. Manser, P. V. Kamat, W. F. Schneider, and M. Kuno, Nat. Commun. **8**, 200 (2017).

[18] Z. Chen, G. Brocks, S. Tao, and P. A. Bobbert, Nat. Commun. **12**, 2687 (2021).

[19] A. J. Barker, A. Sadhanala, F. Deschler, M. Gandini, S. P. Senanayak, P. M. Pearce, E. Mosconi, A. J. Pearson, Y. Wu, A. R. Srimath Kandada, T. Leijtens, F. De Angelis, S. E. Dutton, A. Petrozza, and R. H. Friend, ACS Energy Lett. **2**, 1416 (2017).

[20] E. M. Hutter, L. A. Muscarella, F. Wittmann, J. Versluis, L. McGovern, H. J. Bakker, Y.-W. Woo, Y.-K. Jung, A. Walsh, and B. Ehrler, Cell Rep. Phys. Sci. **1**, 100120 (2020).

[21] I. L. Braly, R. J. Stoddard, A. Rajagopal, A. R. Uhl, J. K. Katahara, A. K. Jen, and H. W. Hillhouse, ACS Energy Lett. **2**, 1841 (2017).

[22] W. Rehman, D. P. McMeekin, J. B. Patel, R. L. Milot, M. B. Johnston, H. J. Snaith, and L. M. Herz, Energy Environ. Sci. **10**, 361 (2017).

[23] H. X. Dang, K. Wang, M. Ghasemi, M. C. Tang, M. De Bastiani, E. Aydin, E. Dauzon, D. Barrit, J. Peng, D. M. Smilgies, S. De Wolf, and A. Amassian, Joule **3**, 1746 (2019).

[24] K. A. Bush, K. Frohna, R. Prasanna, R. E. Beal, T. Leijtens, S. A. Swifter, and M. D. McGehee, ACS Energy Lett. **3**, 428 (2018).

[25] M. B. Johnston and L. M. Herz, Acc. Chem. Res. **49**, 146 (2016).

[26] J. H. Noh, S. H. Im, J. H. Heo, T. N. Mandal, and S. I. Seok, Nano Lett. **13**, 1764 (2013).

[27] A. Ruth, M. C. Brennan, S. Draguta, Y. V. Morozov, M. Zhukovskyi, B. Janko, P. Zapol, and M. Kuno, ACS Energy Lett. **3**, 2321 (2018).

[28] M. C. Brennan, S. Draguta, P. V. Kamat, and M. Kuno, ACS Energy Lett. **3**, 204 (2018).

[29] T. Elmelund, B. Seger, M. Kuno, and P. V. Kamat, ACS Energy Lett. **5**, 56 (2020).

[30] A. Sher, M. van Schilfgaarde, A.-B. Chen, and W. Chen, Phys. Rev. B **36**, 4279 (1987).